university of groningen

faculty of science and engineering

A new calibration for the Darker Skies Sky Quality Camera Network for light pollution monitoring

Alex Hin (s3516539)

university of groningen / faculty of science and engineering

University of Groningen

A new calibration for the Darker Skies Sky Quality Camera Network for light pollution monitoring

Bachelor's Thesis
Bachelor of Science in Astronomy
at University of Groningen under the supervision of
Prof Dr R.F.Peletier (Kapteyn Institute, University of Groningen)
and second reader
Dr. R. Hesper (Kapteyn Institute, University of Groningen)

Alex Hin (s3516539)

August 3, 2025

Contents

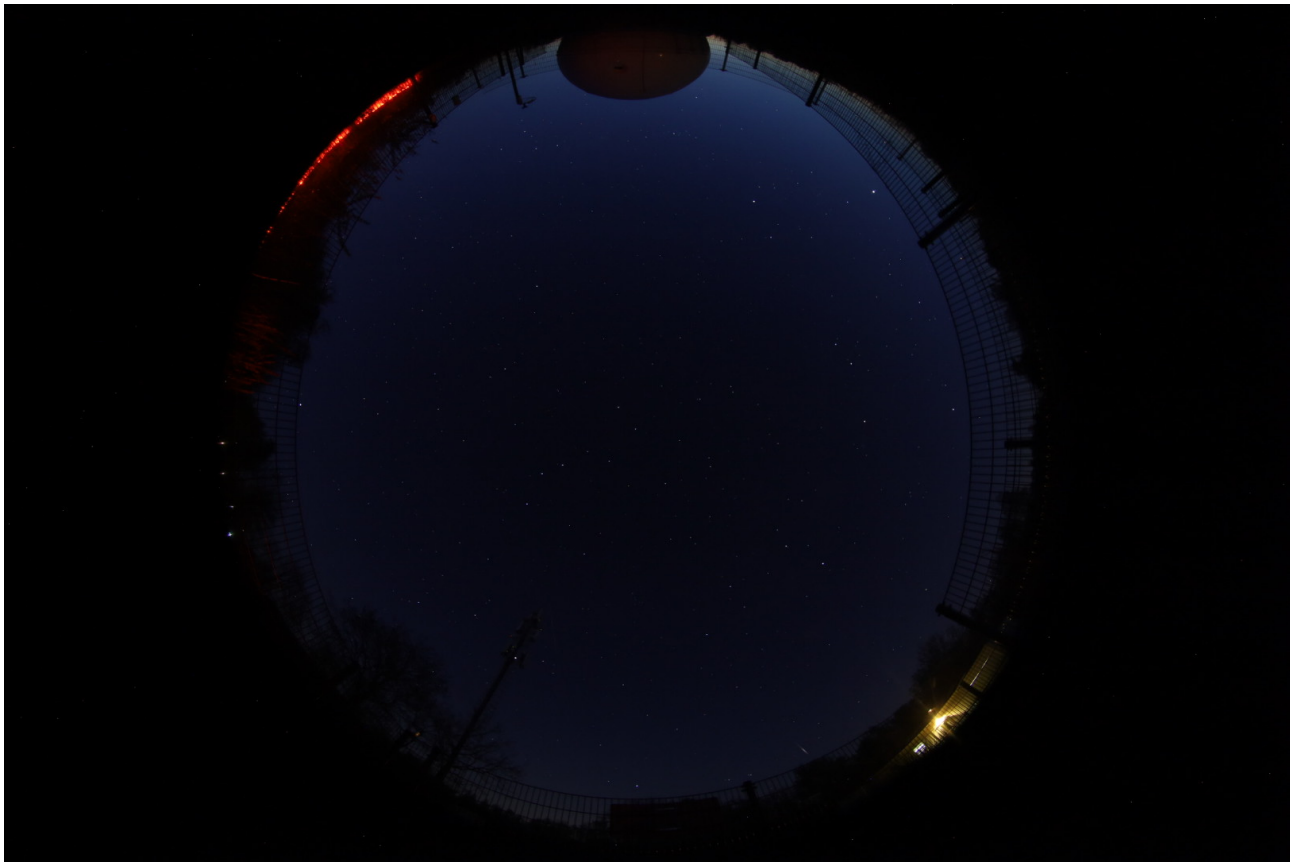

Acknowledgments

First of all, I would like to thank my supervisor, Prof. dr. Reynier Peletier. This has been quite an adventure, but I enjoyed every part of it. The possibility to work in a field I am passionate about and that focuses on a skillset I wanted to improve has been an amazing experience. Similarly, Nynke Visser and Dirk van der Geest for all their help during the project and for answering all my questions.

Second, Dr. Ronald Hesper and Prof. Dr. Andrey Barychev for their availability during my defence and for taking the time to read my thesis. Without you, I would not have been able to complete this and continue to the next chapter of my life.

Third, I would not have been able to do this without my amazing family and friends. Challenges like these can feel daunting, but the support from all these people ever since the first year of my studies is what kept me going. It might not have been the fastest route, but they stood by me and supported me nonetheless. Whether it was sharing beautiful experiences, emotional support or gifting me hundreds of pens to write my exams. It has been the combination of all of you that got me to where I am now.

Abstract

This thesis presents an algorithm for automated photometric calibration of all-sky DSLR camera systems using plate solving. The system calculates instrumental magnitudes in the R, G, and B bands for multiple stars throughout different nights and locations, and are subsequently compared to catalog values from SIMBAD. Photometric zero points and colour terms are derived to correct for systematic offsets and colour-dependent effects. The accuracy of the calibration is assessed through statistical analysis and visualised using calibrated absolute magnitudes for each colour band. The results demonstrate the reliability of using a DSLR camera for quantitative sky brightness and colour index measurements, enabling its use for long-term monitoring of night sky conditions and light pollution.

1 Introduction

The night sky has been plagued with artificial lighting since humans started harnessing the power of electricity. This is very useful for human productivity and sense of safety. However, due to the artificial light creating a phenomenon that we generally call light pollution. The problem stems from the concept of artificial light at night (ALAN). At night, there are significantly fewer natural sources of light. Most of Earth's flora and fauna are adapted to these light sources, like moon cycles and starlight, due to their natural prevalence during the evolution of life. But it comes with a plethora of negative influences. In humans, this can result in the disruption of the circadian rhythm, which links to increases in diseases and problems like obesity, diabetes, heart disease and even multiple types of cancer [Vladimir, 2006] [Cao et al., 2023]. Similarly, flora and fauna can be affected in multiple sectors. Plant growth patterns can significantly change to longer photosynthesis periods due to increased light exposure [Aubé et al., 2013]. Animals that thrive in dimly lit environments see their scavenging grounds severely limited, and bugs get caught indefinitely revolving around lantern poles. These biological effects can significantly impact societies and ecosystems.

In the astronomical world, it makes Earth-based observations more and more difficult [Aubé et al., 2013]. Areas in the world that are densely populated and technologically advanced suffer increasingly from excessive artificial lighting [Pun et al., 2014], meaning that more than 99% of inhabitants of the USA and Europe live under light-polluted skies[Falchi et al., 2011]. The Netherlands can be considered a prime example of such an area. Areas like the Randstad and Westland are the most light-polluted areas in the entirety of Europe, being around 7000 times more polluted than their darkest European counterparts [Falchi et al., 2019]. This makes it hard for telescopes in the Netherlands to research faint objects that can easily be overpowered by nearby light sources. While Groningen has not yet caught up to these levels, it has light pollution simply by having a sizable population. To mitigate this problem in a specific region, it is essential that we first gather information about the current state of light pollution in that region by monitoring various types of locations. This monitoring can shed more light on how to improve lighting conditions and which areas are most impacted by ALAN. With this information, it is possible to start reducing light pollution in affected areas and scientifically present findings to municipalities and governments to start discussions about legislation.

The DARKER SKY [DKS, 2023] project, funded by the Interreg North Sea Programme, is a collaborative initiative aimed at reducing light pollution and enhancing biodiversity and ecological connectivity across the North Sea Region. This collaboration includes France, Germany, the Netherlands, and Denmark. The project runs from April 2023 until October 2026 and, as one of its main goals, aims to provide municipalities and ports with measurements and monitoring in pilot areas. Improvements to monitoring are important, as most information comes from datasets like the NASA Black Marble monitoring. These space-based observations use the Visible Infrared Imaging Radiometer Suite (VIIRS), which has a spatial resolution between 750m to 500m, only monitor in the far R band (500nm-900nm) and do not allow for research around the horizon [Román et al., 2018][Nicotera, 2022]. Working with such a large resolution makes it difficult to make decisions on smaller scales, like reducing lamp posts in neighbourhoods. This is where this thesis comes in. Within the province of Groningen (NL), there are several locations used as pilot sites for monitoring light pollution. The Dark Sky Park Lauwersmeer, harbour of Lauwersoog and the Zernike University complex all have multiple options for measurements. The devices used by the University of Groningen (RUG) at these locations are Sky Quality Meters (SQMs) and Digital single-lens reflex cameras (DSLRs), both serving different purposes that will be discussed in the next part. This thesis will discuss the process of

broadening the toolkit for research on light pollution using DSLRs.

There are multiple ways of finding the sky brightness using ground-based instruments. The Unihedron SQM-LU Sky Quality Meters (SQMs) are commonly handheld devices that function like a simple photodiode sensor that can be brought anywhere. These can also be mounted to function like a basic monitoring station when weatherproofed. This provides an affordable option that constantly measures a small angle for its sky brightness. While perfect for long-term monitoring, there are several limitations to SQMs. Firstly, they only have a limited field of view of 20°, which means that light pollution analysis of areas outside of the region around zenith are impossible. Second, they have a single photometric band, similar to the astronomical V-band, but not equal[Hänel et al., 2018]. Reducing light pollution often focuses on specific source types, like blue LEDs or more orange-leaning sodium lights [Sánchez de Miguel et al., 2017]. This makes the data provided by just SQMs incomplete for precise changes in, for example, lighting type changes.

Since 2023, the Keep It Dark[KID, 2021] (KID) project has introduced a more advanced version of sky monitoring. These are Digital single-lens reflex cameras (DSLRs). The introduction of these cameras has been continued by DARKER SKY to increase the number of monitoring stations available. The pictures taken by these cameras are spread over 3 types of subpixels, red, green and blue. These can be combined into the pictures that we are used to, but when taking their data individually, we can analyse the results in more detail and compare them to known values in the astronomical field. Because the DSLRs are outfitted with fish-eye lenses, it is possible to observe the entire sky from horizon to horizon. While the DARKER SKY Cameras have already compiled years of data, they have yet to be processed, calibrated and analysed to obtain relevant data to complete the mission goals stated by the project.

1.1 Research Questions

To summarize, this thesis focuses on the following problems:

Q1. How can digital cameras be photometrically calibrated to measure the sky brightness of light pollution using observational data accurately?

Q2. Can the calibration of these cameras be automated for further deployment of the network?

Q3. How do the calibrated cameras compare to SQM data in the same area?

Q4. What is the colour of the sky, and how does this change per location?

1.2 Thesis Outline

This thesis presents a workflow for automated measuring and analysing night sky brightness and colour using consumer digital cameras. The main goals are to assess the accuracy of such cameras for photometric monitoring, understand calibration uncertainties, and study how sky brightness and colour indices change over time.
The methods include automated data collection from wide-angle cameras, raw image processing, astrometric calibration using plate-solving, and photometric calibration by matching detected stars to catalog values. Instrumental magnitudes are measured via aperture photometry, and photometric

zero points are determined by comparing stars to SIMBAD catalog magnitudes. Time series of sky brightness and colour indices are constructed and compared with standard SQM measurements.
Results show reliable star identification, robust calibration, and agreement with reference data. Trends in sky brightness and colour indices are analysed as a function of time. The approach enables continuous, multi-site monitoring of night sky conditions.
The thesis concludes with a summary of contributions and suggestions for improving calibration and expanding the monitoring network in future work.

2 Methods

2.1 The cameras

All-sky images were collected using a Canon EOS R DSLR Camera with a 35.9 x 24.0mm sensor with 6240 x 4160 pixels, resulting in a subpixel group the size of around 5.76 μm. Attached to the camera is a Canon EF 8-15mm f/4.0L Fisheye lens. It is placed on a solid structure, meant to keep it steady over time. The camera and its Single-Board Computer (SBC) are housed in a weatherproof enclosure, allowing them to exchange sufficient heat with the environment and remain dry in rainy or humid conditions as seen in figure (1). The fisheye lens creates a radial projection that is dependent on the model of the lens[Yin et al., 2025]. These distortion effects are explained by [Kannala and Brandt, 2006] and become more important the further to the horizon measurements are done. The entire construction utilises grid power to keep all components powered and running indefinitely. Units are installed at the Zernike Campus (Groningen), Lauwersoog Dark Sky Park, and Lauwersoog Harbour, the first two of these locations have two cameras collecting data using different file formats. The different camera formats are raw image files in the .cr2 or .cr3 format, which were stored locally on the SBC. Once per day, these images are sent wirelessly to the data servers of the Kapteyn Institute. The cameras were turned on on different dates and some have seen downtime during their current lifespan, which can be seen in Table [2].

Figure 1: SQC unit as used at the Dark Sky Park Lauwersmeer location.

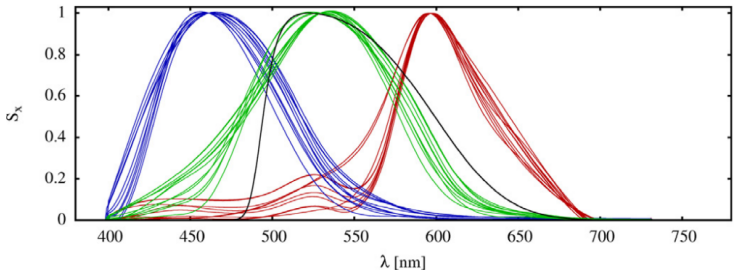

Figure 2: Passband response curve of similar DSLR cameras as used in this thesis[Kolláth et al., 2020]

There is an overlap in these types of pixels as they take in a broad spectrum of light, as seen in figure (2). Shown here are the spectral response curves of several cameras of similar type as the EOS R used in this study. The black line indicates the astronomical V band. Here we can see that the green filter is centred around 550nm (5500Å). Similar to the human eye, which ranges from around 400-700nm. [Sánchez de Miguel et al., 2019]

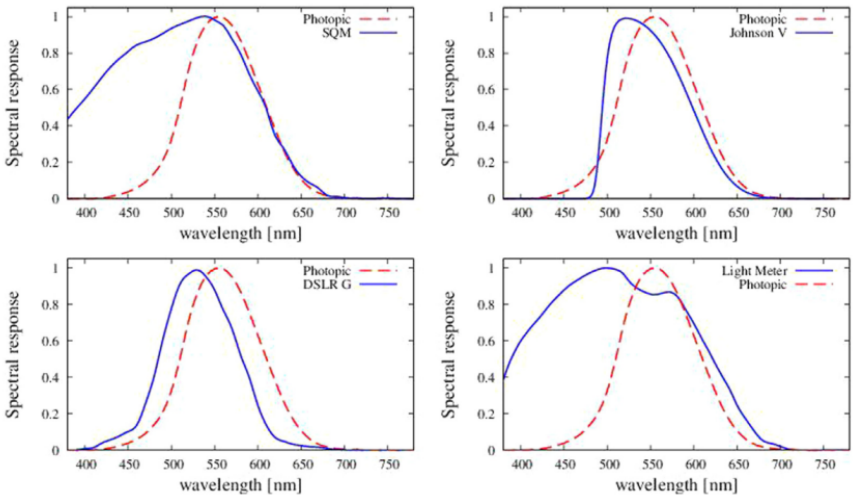

Figure 3: Spectral response of several observation devices and filters, compared to the human eye's photopic vision [Hänel et al., 2018]

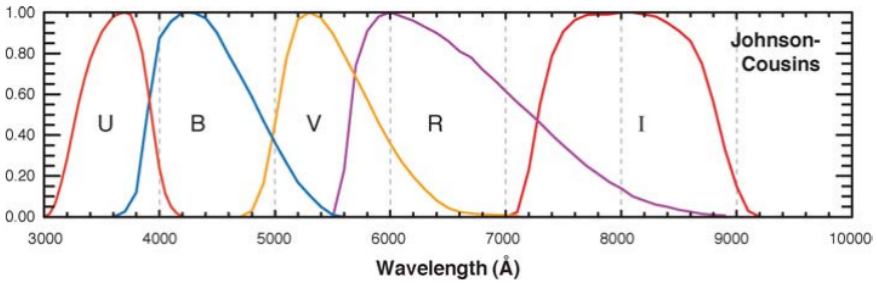

Figure 4: The typical response curve of the Johnson-Cousins UBVRI System[Bessell, 2005]

In figure 4, the Johnston-Cousins bands are plotted. When we compare these to the response curves from figure 3, there is a large difference in the spectral response of each instrument that needs to be corrected.

2.2 The SQM

The SQM data is compared to comes from a Unihedron SQM-LU, where the data is stored on Washetdonker.nl. This SQM uses the TSL237 light-to-frequency converter combines a silicon photodiode and a current-to-frequency converter on a single monolithic CMOS integrated circuit. The output is a square wave (50% duty cycle) with frequency directly proportional to light intensity on the photodiode[Cinzano, 2005]. The digital output allows direct interface to a microcontroller or other logic circuitry. The device has been temperature compensated for the ultraviolet-to-visible light range of 320 nm to 700 nm (figure 3)

	$\lambda_B(nm)$	$\lambda_G(nm)$	$\lambda_R(nm)$
Johnston-Cousins [Bessell, 2005]	436.1	544.8	640.7
DSLR [Kolláth et al., 2020]	460	530	590
SQM [Hänel et al., 2018]	-	550	-

Table 1: Effective wavelengths of each RGB system

The effective wavelength of each system are referenced in table 1

2.2.1 Date Selection

Finding data applicable in the Netherlands is rather hard, but by using a small Python loop, it was possible to extract data from WasHetDonker [WAS, 2019], which showed the magnitude curve for the entire evening. This made it easier to loop across the different days and find suitable options.

Depending on the camera, the images made are either in the Canon Raw Version 2 (.cr2) or Canon Raw Version 3 (.cr3) format. Both files employ a lossless compression algorithm, and for the purposes of this thesis, the difference in file type does not matter. The integration time of all cameras is currently standardised to 30 seconds. After that, the camera waits for 2 minutes and takes the next image.

camera	**location**	**file type**	**starting date (yyyy-mm-dd)**
Zernike_SQC	Zernike Campus Groningen	.cr2	2023-08-12
Zernike_EOSRP	Zernike Campus Groningen	.cr3	2023-10-01
Lauwersoog_SQC	Dark Sky Park Lauwersoog	.cr2	2023-11-17
Lauwersoog_EOSRP	Dark Sky Park Lauwersoog	.cr3	2023-08-17
Port_EOSRP	Lauwersoog Harbour	.cr3	2024-02-09

Table 2: camera overview

To select observing dates, similar to[Kolláth, 2010], we try to find a night where:

- All locations have at least 1 camera running (see table 2)
- The moon is not present above the horizon for the duration of the camera's imaging cycle.
- Weather conditions are applicable for astronomical observations, meaning no clouds, rain or other weather effects.
- There is a long period beyond astronomical twilight, i.e. in which the sun is at least 18 degrees below the horizon

2.3 Data gathering and processing

2.3.1 Raw image handling

Raw images were processed using the rawpy Python library, which allows direct access to the Bayer matrix data. This matrix is a 2x2 group of pixels, following the order red, green then green, blue. Knowing this made it possible to separate the raw image into its red, green, and blue channels by indexing the Bayer matrix with a function as seen in figure 5.

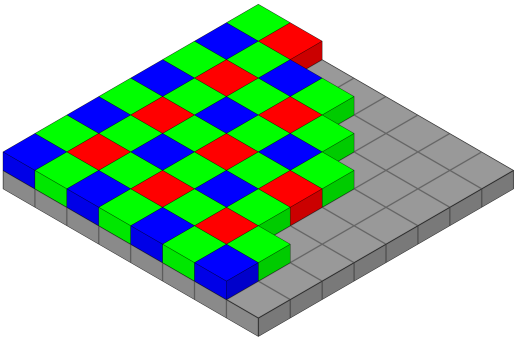

Figure 5: typical Bayer matrix like in the Canon EOS R DSLR Camera

The green channel was computed as the average of the two green pixels in each Bayer block, which improves the signal-to-noise ratio for the green measurements. Red and blue have only half of the pixels of green due to this matrix setup, which can make measurements noisier.

2.3.2 Astrometry

To calibrate the cameras and compare data with other sources, it is mandatory to find a proper magnitude for the stars in the picture. To do this, we use a concept called plate solving, a coordinate transformation from cartesian pixel grid to the equatorial sky coordinates, specifically Astrometry.netLang et al. [2010]. After selecting a clear night, a picture was taken during the middle of the night, and stars were visible. Slicing to an area of 800x800 pixels around the centre, this frame was converted into a .fits file, an image file type that Astrometry.net can handle.

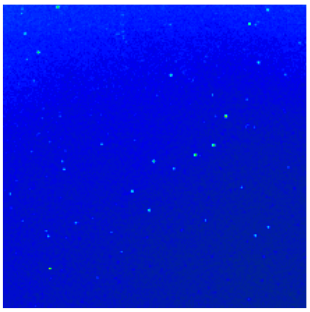

Figure 6: Example fits file converted from the center of the image. Made with the Zernike_SQC over showing Ursa Major

2.4 Astrometric calibration and star catalog matching

Astrometric solutions for the images were obtained using the Astrometry.net client [Lang et al., 2010], which produced FITS files with World Coordinate System (WCS) headers. These headers allow for the transformation between pixel coordinates and celestial coordinates (RA, Dec). This is also how the zenith for a camera can be determined from its location. This technique was first provided by Greisen & Calabretta [Calabretta and Greisen, 2002] and is used widely in astronomy.
Astrometry provides several options for successfully identified images, of which the corr.fits is the catalog of detected sources, but some information was still lacking. The stellar magnitudes are only given for a single colour channel as the fits file is only of one colour, and no identifier (i.e. name or designation) were given for bright stars. To begin calibration and automating this, a subset of all objects needed to be selected. Bright stars (magnitude 0–4, according to Astrometry) were selected from the catalog for calibration. Their celestial coordinates were cross-matched with the SIMBAD database using astroquery. Simbad hosts a large amount of celestial data that can be interfaced within Python. This makes the automatic calibration for any camera at a given location possible on any given time. Stars that could get matched by astroquery were appended with names, zenith distance, airmass and literature values for R, G, and B magnitudes. This matching was performed automatically for all stars in the field, using a search radius of 50 arcminutes and a magnitude criterion (G $<$5) to ensure reliable identification. Stars unable to be

matched by this process were discarded to avoid the need for manual tuning of the calibration. Out of the 16 to 18 stars that were usually found in the magnitude filter, 2 or 3 could not be matched this way.[Ducati, 2002][Cardiel et al., 2021]

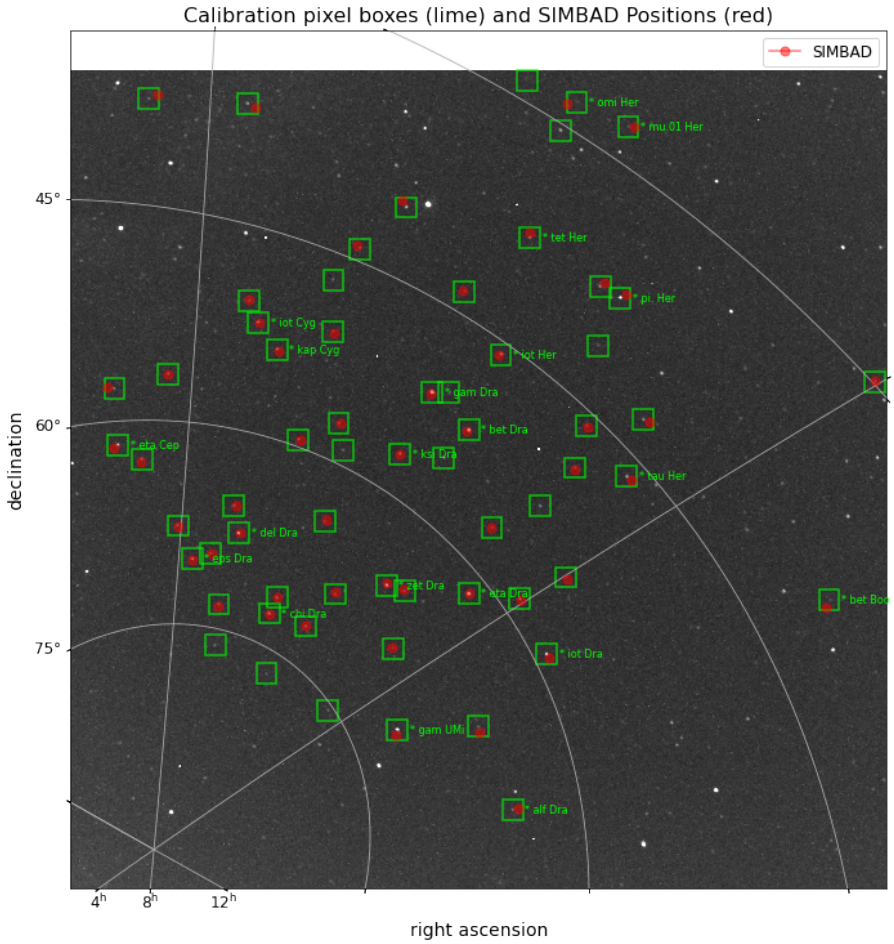

Figure 7: The location of all stars found for one evening by astronomy.net highlighted with lime boxes. Objects found near these locations are marked with red and could have star names attached if found for that specific location.

2.5 Photometric Calibration

2.5.1 Instrumental magnitude measurement

For each calibration star, its pixel position was determined using the WCS solutionCalabretta and Greisen [2002]. The measure_star_flux function extracted a cutout around the expected position and performed aperture photometry using the photutils package. The background was estimated from an annulus around the star, and the net flux was converted to an instrumental magnitude using the standard formula:

$$m_{inst} = -2.5 \log_{10} \left(\frac{F_{\text{star}} - F_{\text{bkg}}}{t_{\text{exp}}} \right) \quad (1)$$

where in equation(1) (m_{inst}) is the instrument magnitude of the system, (F_{star}) is the total flux or intensity in the aperture, (F_{bkg}) is the estimated background flux, and (t_{exp}) is the exposure time[Bessell, 2005][Hearnshaw, 1996].

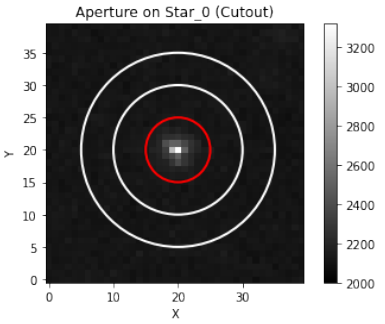

Figure 8: Example of the photometry used to obtain the flux of each star

2.5.2 Star tracking across frames

To account for field rotation and tracking, the code calculated the expected pixel shift of each star between frames based on the change in right ascension using the get_star_pixel function. The G band was used to accurately determine the location of the star, and this location was used for both red and blue images, as the noise from these bands made tracking unreliable. This allowed consistent tracking of stars across multiple images, even as the sky shifts as the Earth revolves during the night. We can use multiple calculations of stars to lower the error value in our magnitude, the relation between distance and magnitude or camera consistency.

2.5.3 Zero point determination

Instrumental magnitudes were compared to SIMBAD catalog values for each filter (R, G, B). The photometric zero point for each band was computed as the mean difference between catalog and instrumental magnitudes for all calibration stars with valid measurements. Outliers of $\pm 3\sigma$ are excluded using a sigma-clipping approach. The zero points were then used to calibrate the initial instrumental magnitudes to the standard system to star observation. By combining the different values for magnitude over multiple frames, the error of the zero point magnitude can be established. This is done for every single colour band over all stars.

2.5.4 Bias and colour terms

To correct for detector bias, the system determines the length and width of the image to identify the parts of the camera that are not used for imaging the surrounding environment. The columns mean of each image (representing the detector's dead zones) were calculated and subtracted from the science region. This step ensures that the measured fluxes are not affected by electronic offsets in the detector. The system can't compensate for a dark current in the camera, as the device would need to be automated to remotely cover itself temporarily. This is not strictly necessary for the calibration, but it is mandatory when measuring the sky brightness over the night.

Another factor that needs to be corrected for is the colour term, as the camera is not perfectly aligned to the response curve of the data obtained by SIMBAD. We know their effective wavelengths are B = 450 nm, G = 555 nm, R = 670 nm[Ducati, 2002], which are spread out to the far end of the RGB spectrum used by the camera. To compensate for this, we use linear regression on our instrumental magnitudes to obtain improved zero-point measurements. The calculation gives us a formula like: $\Delta mag = zp + C(B-V)$ where zp refers to the zero point and C is the colour term compensation for a star's b-v term. Correcting for both is used to more accurately predict the zero point of the camera and how to correct for red or blue stars.

2.5.5 Determining the sky background

A circular mask was generated to select the region within 10 degrees of the zenith, using the maskMaker function. This function takes any one image on the camera and the zenith pixel from the WCS. A boolean mask corresponding to the desired angular radius was created. The slicer2 function then summed the pixel values within this mask for each colour channel, providing a measure of the sky brightness near zenith. This process was repeated for all images in a given night, resulting in a time series of sky brightness in each colour channel. Initial computing methods required the scanning of included pixels on a per-image basis. It was too computationally heavy to calculate using this method, resulting in the program taking several hours to complete the data. The second implementation using the mask made the computation significantly faster, going down to just 2-3 minutes, which proved incredibly helpful.

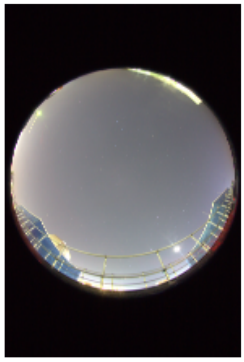

Figure 9: Example image showing that bias can be obtained from using image borders

2.6 Time series and colour analysis

The sky brightness in each colour channel was tracked throughout the night by processing all images in a given folder. The results were stored in a dataframe and saved for later analysis. The calibrated sky brightness was compared to external measurements from the WasHetDonker SQM network, allowing for validation of the photometric calibration.
Color indices (B–V, V–R) were computed for each time point, and their evolution was plotted to study atmospheric and environmental effects, such as extinction and colour patterns. The colour indices were also used to investigate the stability of the photometric calibration and to identify any systematic trends.

2.7 Visualization

All data processing and visualization were performed in Python using matplotlib, astropy, and photutils. Star positions, sky regions, and calibration results were visualized on the FITS images using WCS projections, with annotations for star names and zenith position. Time series plots of sky brightness and colour indices were generated to illustrate the temporal evolution of the night sky conditions.

3 Results

3.1 Star identification and astrometric data collection

To demonstrate the program's capabilities for calibration and monitoring, data from all three locations were used on the night of June 20, 2025, using the three EOSRP cameras. This date is very close to the summer solstice, meaning the sun never reaches the preferred angle of -18°altitude. Still, due to either camera defects, weather issues or other circumstances, it was the best solution for monitoring a single day across all cameras. Before this, however, we can observe the results from 25-04-2025, where the night is significantly longer and the sun does pass -18°altitude. For brevity in this section, we omit the data from the Zernike Campus and Lauwersoog harbour on 20-06-2025, but these can be found in the appendix.
Stars were automatically cross-matched with the SIMBAD database using their coordinates, retrieving their main identifiers and literature R, G, and B magnitudes. Figure 10 shows representative FITS images with the WCS overlay, the zenith position marked, and all calibration stars annotated by name. The yellow circle indicates the region within 10 degrees of zenith, which was used for sky brightness measurements. The contrast between stars and the night sky is high due to the low altitude of the sun.

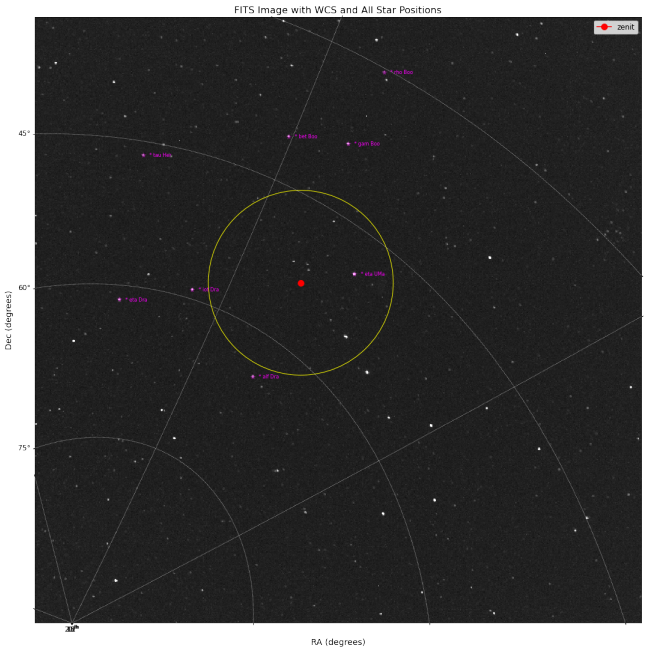

Figure 10: The overview of stars used by the program for calibration. Indicating the stars, the zenith point of the image and the 10 deg radius used for night-long analysis.

3.2 Photometric Calibration

For each star in the plate-solved FITS file, instrumental magnitudes in the R, G, and B bands were measured using aperture photometry, with local background subtraction via an annulus. R_{inst}, G_{inst}, B_{inst} were determined as the median of sigma-clipped measurements across multiple frames to reduce the impact of outliers and noise, with usually around 10 to 15 measurements. Only stars with both reliable SIMBAD and instrumental magnitudes were used for calibration.

To account for colour-dependent systematics, the difference between instrumental and SIMBAD magnitudes was plotted against the SIMBAD $(B-V)$ color index for each band. A linear regression was performed:

$$m = m_{inst} + a + c \cdot (B-V) \tag{2}$$

where a is the instrumental zero point of the system and c is the colour term coefficient. This allowed for the correction of both colour-dependent offsets in the instrumental system and the compensation for the instrument's zero point.

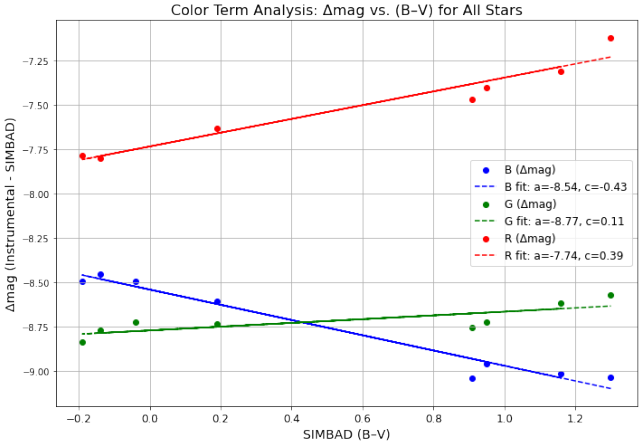

Figure 11: colour term calibration across stars in different bands

Combining these values, we can derive the magnitude for each star as seen in figure 12.

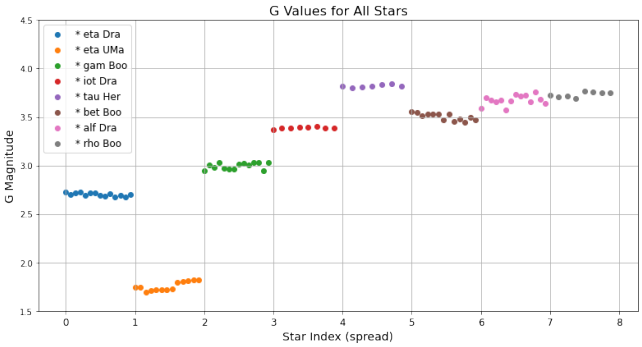

Figure 12: Stellar magnitudes, derived from the instrumental magnitude and zero point determination on 25-04-2025 at Dark sky park Lauwersoog

Stars can now be compared to literature values, as all stars have obtained the apparent magnitude according to our system2. To check for systematic errors or biases in each colour band and quantify the agreement between instrumental and catalog magnitudes. In such a way, we can identify outliers or stars with unusual behaviour.

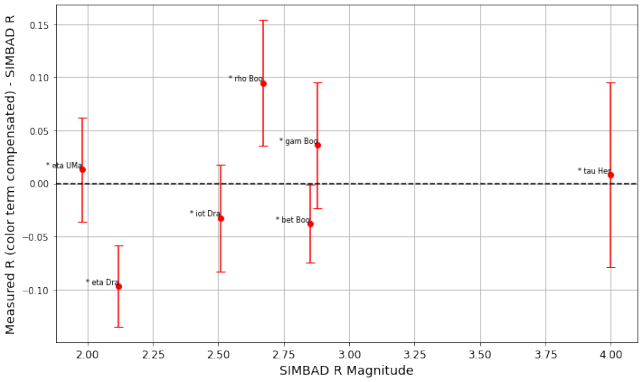

Figure 13: Relationship between calibrated accuracy and absolute magnitude of the star in band R

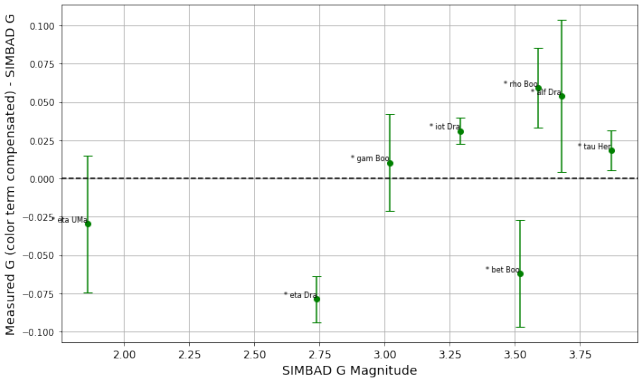

Figure 14: Relationship between calibrated accuracy and absolute magnitude of the star in band G

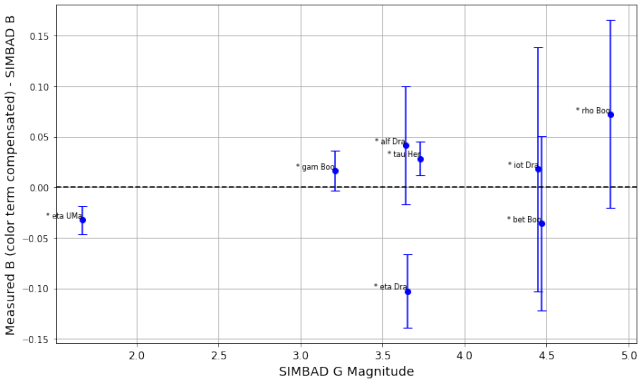

Figure 15: Relationship between calibrated accuracy and absolute magnitude of the star in band B

While we can see in figure 14 that the error margin in the green band is better than red (f13) or blue (f15) due to the higher S/N ratio of the green pixels in the Bayer matrix.

3.3 Individual Star Tracking

To assess the photometric stability and calibration quality of the camera system, the instrumental magnitudes of a reference star (eta Dra) were measured throughout the night. It computes the mean

and standard deviation of the measured R, G, and B magnitudes, applies the previously determined photometric zero points, and plots the resulting calibrated magnitudes as a function of time. Additionally, the angular distance of the star from the zenith is plotted on a secondary axis to visualise any correlation between airmass and measured brightness. Statistical summaries, including colour indices (B–G and G–R), are annotated directly on the plot for reference. This approach provides a clear visualisation of both the photometric accuracy, the effects of changing airmass and other weather anomalies throughout the observation sequence.

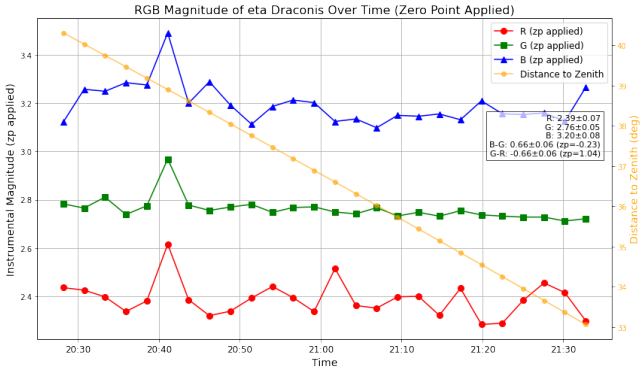

Figure 16: Long term star (eta Draconis tracking on different nights)

3.4 Sky brightness time series around zenith

To evaluate the third research question, the evolution of colour indices and the camera's sky brightness measurements were compared to those from an SQM in the same location. These results are compensated for by the colour term of the sky itself and the zero points determined by the calibration of the system as done above.

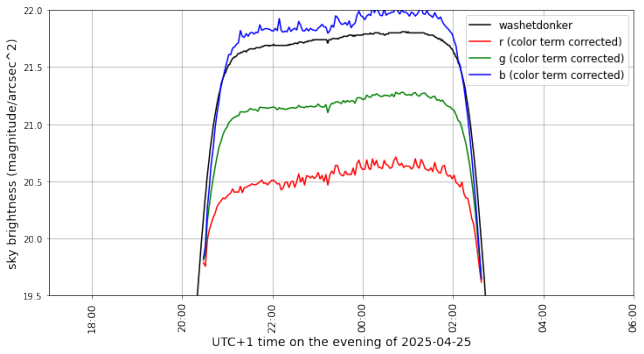

Figure 17: Comparison of Camera-Derived and SQM Sky Brightness at Lauwersoog: Time series of sky brightness in R, G, and B bands from the camera, plotted alongside SQM (washetdonker) measurements.

As seen in the comparison of the response curves of our instruments (figure 3), the SQM has a spectral response that corresponds to DSLR G combined with higher wavelengths, where the B band would be. This corresponds with the results of figure 17 as the SQM is situated between the B and G bands of our system. The R band sits well below the other bands, meaning that throughout the night, the sky is heavily more illuminated in lower wavelengths. With the sun at a maximum altitude of approximately -20°there is still a lot of Rayleigh scattering occurring during the night, making red the

dominant while higher wavelengths get scattered.

To answer our fourth research question about the colour of the sky, we calculate the terms using the compensated magnitudes in each band.

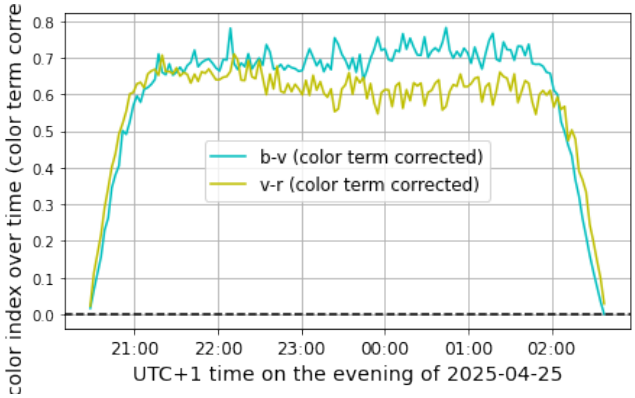

Figure 18: Colour profile of the sky over the night of 25-04-2025. cyan

Subsequently, the camera's R, G, and B magnitudes are interpolated to the SQM timestamps and directly compared to the SQM measurements. The resulting Δmag (Camera – SQM) plot highlights any systematic offsets or trends, serving as a diagnostic for both absolute calibration and temporal consistency. These analyses are essential for validating the reliability of the camera system for night sky brightness monitoring.

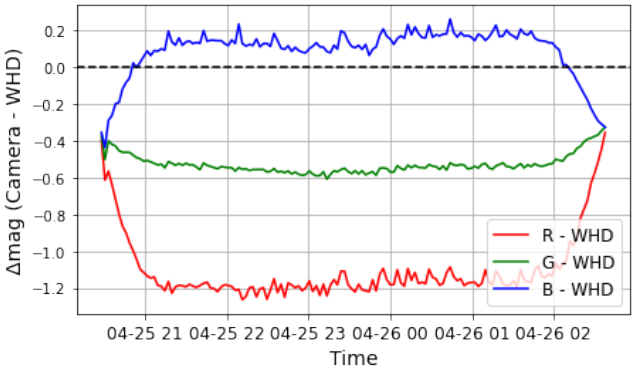

Figure 19: Colour profile comparison with SQM data, where we can see the differences in colours over the night. Shorter wavelengths follow the pattern of the SQM, while longer wavelengths diverge during the darkest moments of the night.

3.5 triple location calibration during prolonged sunset on 20-06-2025

To compare these numbers and examine trends among different stations, we turn to June 20th 2025, when all stations were running during clear weather, but without astronomical twilight.

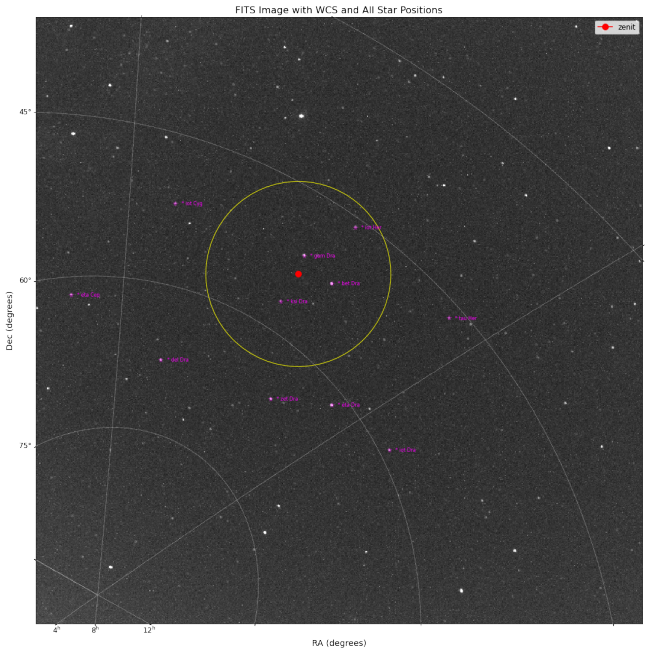

Figure 20: The overview of stars used on Juli 20th. Indicating the stars, the zenith point of the image and the 10 deg radius used for night-long analysis.

The S/N during prolonged sunset is visibly higher in figure 20, resulting in noisier calibration values for each star.

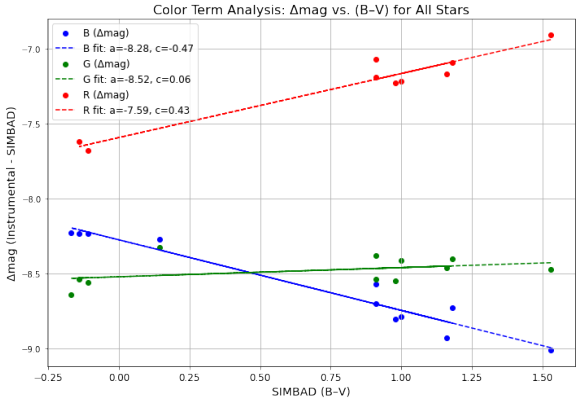

The colour term profile of the lauwersnest camera

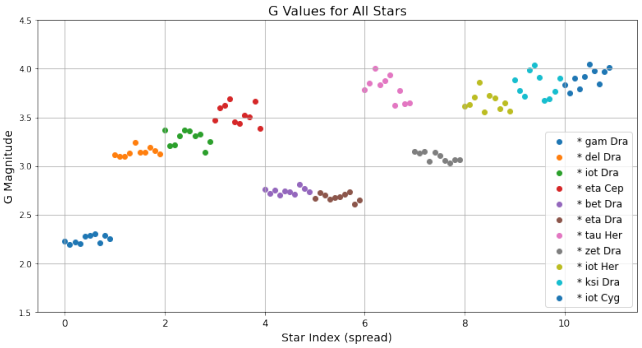

Stellar magnitudes, derived from the instrumental magnitude and zero point determination

Figure 21: Color term and zero point determination on July 20th

As expected, figure 21 shows that the system has significantly more noise during nights closer to the summer solstice.

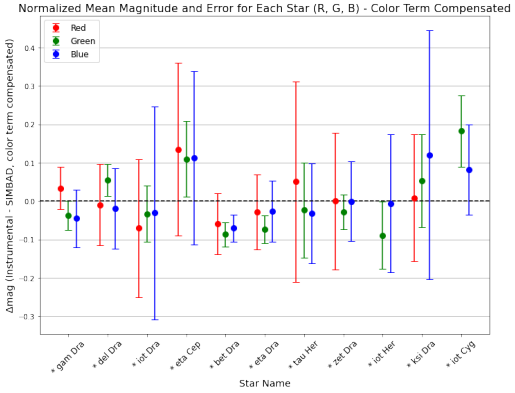

Color compensated absolute magnitudes of the calibration stars.

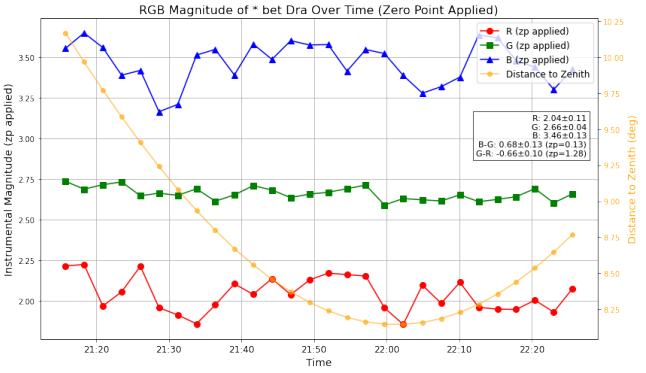

Single star tracking over longer periods. While the star approaches its closest point to zenith, there is no clear change in observed magnitude due to airmass.

Figure 22

Location	zp_R	zp_G	zp_B
Port (Port EOSRP, 2025-06-20)	7.389 ± 0.0922	8.354 ± 0.0900	8.078 ± 0.0863
Lauwersnest (Lauwersoog EOSRP, 2025-06-20)	7.594 ± 0.0630	8.523 ± 0.0870	8.276 ± 0.0732
Zernike (Zernike EOSRP, 2025-06-20)	6.687 ± 0.192	7.595 ± 0.202	7.329 ± 0.176

Table 3: Photometric zero points (zp) and uncertainties for each camera location and band.

Table 3 summarises the final calibrated magnitudes for each star in the R, G, and B bands. This overview forms the basis for evaluating the performance of the camera and its accuracy as a tool for light pollution measurements.

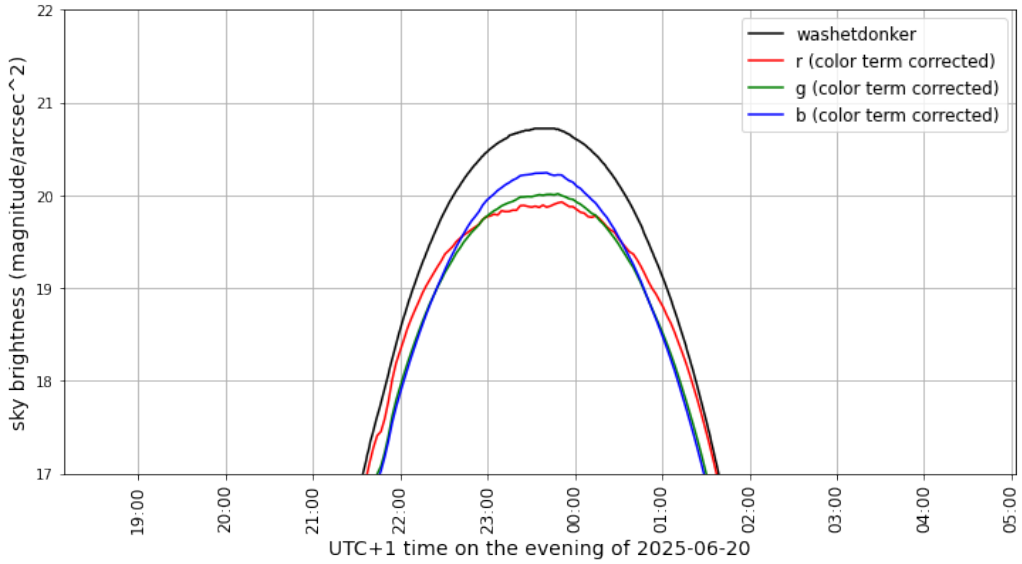

Figure 23: Full night sky brightness profile of all three colour bands (R,G,B), compared to SQM readings at the same location (black) during Juli 20th

The sky brightness time series around zenith in figure 23 looks very different compared to April, as expected. The sun barely sets close to the summer solstice and the light of the sun reaches the camera throughout the night. During the darkest part of the night, longer wavelengths still obtain the most light, hinting at Rayleigh scattering in a similar sense to the earlier example

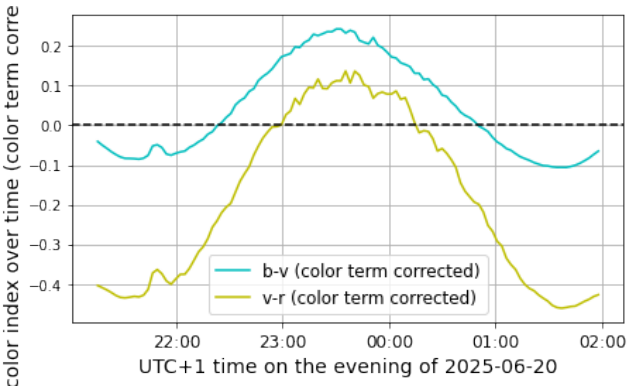

Colour term analysis of the sky over night

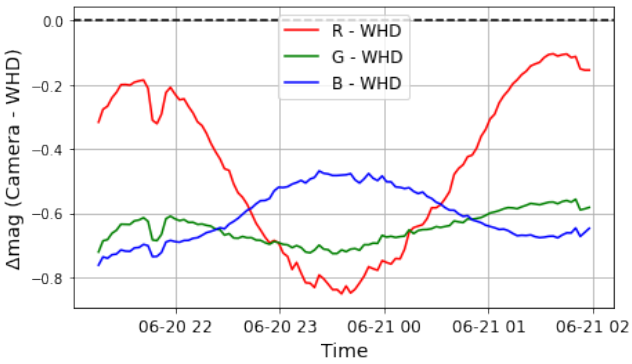

Colour profile comparison between SQM data and DSLR, where we can see the differences in colours over the night.

Figure 24: Sky colour measurements during prolonged sunset

In figure 24, it is visible that Shorter wavelengths trend positively to sunset, while longer wavelengths diverge during those darkest moments. This is similar to our findings in April, although the gap between blue and green is significantly larger.

4 Discussion

4.1 Astrometric and photometric calibration

The use of Astrometry.net for plate solving proved effective for establishing a World Coordinate System (WCS) solution for each FITS image. This enabled accurate mapping between pixel and celestial coordinates, which is essential for both star identification and photometric calibration. Later, it was found that there is a specific function in astroquery that also interacts with Astrometry.net (astroquery.astrometry_net). This can be looked into to make the code more self-sufficient. However, there was no time to look into this for now. The automated cross-matching with the SIMBAD database allowed for efficient retrieval of literature magnitudes for most bright stars in the field. However, a small fraction of stars could not be matched, likely due to positional uncertainties, rounding errors or a field of view that was too wide to accurately convey the precise RA or Dec of the star. This slightly reduced the sample size for calibration. Therefore, the scope of stars might be increased by searching for options further from the zenith and of lower intensity. Matching these is more complex, but can result in a significant increase in accuracy. It is also noteworthy that the function in charge of tracking a star required some assistance. The WCS alone was not enough to keep track of the star in a consistent manner over long periods.
The photometric calibration process, based on aperture photometry and background subtraction, yielded zero points for each band (R, G, B). The scatter in the zero point was smallest for the brightest stars, as expected due to higher signal-to-noise ratios. However, the drift over multiple frames makes determining a zero point only viable for a short number of follow-up frames. This highlights the importance of accurate tracking, selecting calibration stars with high S/N and reliable catalog magnitude matching. It is also visible from figures 13,14,15 and 22 that the spread in the R and B bands was also larger than the G band, resulting in larger error margins for the stars. It could be interesting to see how these values change when using a camera with a different subpixel layout.

4.2 Dependence on airmass and colour term

Analysis of the difference between instrumental and catalog magnitudes as a function of angular distance from zenith showed minimal trends within 10 degrees of zenith. This suggests that, as expected, for the central region of the field, atmospheric extinction is not a significant source of error. For stars further from zenith, a slight increase in Δmag was observed, consistent with increased airmass and possible optical effects at the edge of the field. However, because of the selection, there were few stars selected at these distances. This is in line with expectations from atmospheric extinction theory, where the path length through the atmosphere increases with zenith angle. Airmass calculation is part of the calibration program, so this could be included during further development.
In the photometric calibration of the camera system, we compared the instrumental magnitudes measured in the R, G, and B bands with the reference magnitudes from the SIMBAD catalog. The resulting linear trends indicate the presence of a colour term in each filter. This means, as discussed, that the response of the camera system is not perfectly matched to the SIMBAD photometric system, and the measured magnitude offset depends on the colour of the star. The slope of the fitted line (the colour coefficient) quantifies this effect: a non-zero slope shows that bluer or redder stars are systematically offset in the instrumental system compared to the standard system. This implies that the transformation from instrumental to standard magnitudes requires not only a zero-point correction but also a colour correction term.
The presence of a colour term is expected due to differences in filter transmission, detector sensitiv-

ity, and atmospheric effects. Applying the derived colour term corrections improves the agreement between the camera and catalog magnitudes, as shown in the normalised residual plots.

4.3 Sky brightness and comparison with SQM

The time series of calibrated sky brightness in R, G, and B bands closely followed the simultaneous measurements from the WasHetDonker SQM network. The agreement between the camera and SQM data demonstrates a reliable photometric calibration and the potential of the system for continuous sky monitoring. Some systematic offsets between the camera and SQM readings were observed, which may be attributed to differences in spectral response, filter characteristics, or local environmental effects (e.g., blue light pollution from LED lighting) as mentioned in the methods section. However, the calibration constant of one camera isn't likely accurate for similar cameras. This makes it important that each camera has its own calibration process to make observations as accurate as possible.
It is difficult to make accurate assumptions about the colour difference of nightly observations, as we can see that there is a large variation in different bands. It should be important to continue this research in different areas and dates to see if similar trends are observed and how they are affected by different types of ALAN.

4.4 Colour indices

Colour indices vary significantly over the night. During prolonged sunset, this can be attributed to Rayleigh scattering, which highlights its impact on lower wavelengths. If the calibration process and observation are performed on even more nights, locations and weather patterns, there might be more to say about the significance of the colour indices and how this helps light pollution development.

4.5 Limitations

Several limitations were encountered during the project, mostly regarding time constraints in the development stage of the thesis project. First, a more stable type of star tracking should be included. This should regard the position of the star continuously throughout the night from hopefully just one WCS. The current system can do this accurately for time ranges between 20 and 60 minutes, depending on the star's brightness. The difficulty lies in the resolution of the camera, which is currently around 300 arcsec/pixel. Second, the accuracy of the zero point calibration is limited by the number and quality of calibration stars, as well as the precision of the SIMBAD catalog matching. Third, the system's sensitivity to environmental factors (e.g., clouds, artificial lighting) can introduce additional scatter in the measurements. Fourth, the system set-up might require additional features when observing at lower angles, such as the horizon. This has currently not been tested and may require additional offsets that account for the distortion of the fisheye lens or cap on top of the camera. Fifth, the WCS is currently only applied to the section of the sky around zenith from which the FITS file has been cut out. Going further from the zenith might require more help to accurately determine celestial coordinates. Additionally, integrating real-time weather and seeing data could help interpret variations in sky brightness and colour indices better.

5 Conclusion

5.1 Summary of main contributions

5.1.1 Automated wide-field photometric pipeline, astrometric calibration and star matching

An automated Python pipeline was developed for wide-field photometry using consumer-grade all-sky cameras, considering flexibility for implementing new locations. The pipeline is designed to process raw camera data, perform astrometric and photometric calibration, and monitor night sky brightness with minimal manual intervention.
Astrometric calibration is performed using Astrometry.net, providing relatively accurate World Coordinate System (WCS) solutions for each field. Detected sources are automatically cross-matched with the SIMBAD database to retrieve literature magnitudes (R, G, B) and identifiers for calibration stars. This enables robust star identification and does not require manual catalog matching.

5.1.2 Aperture photometry and multi-band calibration

Aperture photometry is carried out for each calibration star in the R, G, and B bands using the photutils package. For each star, a cutout is extracted around its expected position (as determined by the WCS), and the flux is measured within a circular aperture. The local background is estimated using an annulus, and the net flux is converted to an instrumental magnitude. This process is repeated for all suitable calibration stars and several consecutive frames, allowing for solid statistics and outlier rejection via sigma-clipping.

5.1.3 Zero point determination, colour term and error analysis

Instrumental magnitudes are compared to SIMBAD catalog values for each filter. The photometric zero point for each band is calculated as the mean difference between catalog and instrumental magnitudes for all calibration stars with valid measurements. Colour terms for the camera filter are obtained and corrected for with each star. The scatter in the zero-point determination is typically below 0.1 mag for the brightest stars, increasing for fainter stars due to lower signal-to-noise ratios. For each location and night, the zero points and their uncertainties are reported, and the calibration is validated by plotting the difference between camera and catalog magnitudes for all stars and colour bands.

5.1.4 Sky Brightness Monitoring and validation

The pipeline measures and tracks calibrated sky brightness throughout the night in all three bands. These results are directly compared with professional SQM data from the same locations. The close agreement between the camera-derived and SQM sky brightness validates the calibration approach and demonstrates the system's utility for continuous night sky monitoring. Differences between the SQM and DSLR data can be noticed and change depending on the observation date. These differences are likely differences in spectral response and seasonal colour patterns.

5.1.5 Time series and color index analysis

Time series of sky brightness and colour indices are produced for each night and location, revealing atmospheric and environmental trends. The system demonstrates sensitivity to changes in sky conditions, including clouds and artificial light, as reflected in both the absolute brightness and colour indices.

5.1.6 Open and reproducible workflow

All processing steps, from raw data ingestion to final plots and tables, are implemented in Python using open-source libraries such as Astropy, Photutils, and Astroquery. The workflow is fully documented and reproducible, enabling other researchers and citizen scientists to apply the same methodology to similar datasets.

5.2 Future work

While this project demonstrates a robust workflow for automated photometric calibration and night sky monitoring, several avenues remain for further research and improvement:

5.2.1 Airmass and extinction modeling

The airmass correction in this project uses a simple sec(z) model, but it is not applied due to time constraints. More advanced modeling could include real-time atmospheric data (humidity, aerosol content, etc.) or multi-night extinction monitoring to improve the accuracy of extinction corrections, especially in the blue. It is also important to note that working with data close to the horizon likely requires an extension or recalibration of the WCS

5.2.2 Expanded calibration star catalog

Increasing the number of calibration stars, especially fainter ones or those unsolved by astrometry, could improve the robustness of the zero point determination. Cross-matching with other modern catalogs may provide more precise reference magnitudes and colours.

5.2.3 Automation and real-time Processing

While much of the workflow is automated, some steps (e.g., plate solving and manual inspection of outliers) still require user input. Developing a fully automated pipeline resolving these issues would enable real-time sky quality monitoring and alerting. Implementing machine learning algorithms could improve star identification in crowded or noisy fields and automate the rejection of problematic frames (e.g., those affected by clouds or technical issues).

5.2.4 miscellaneous topics

The residual analysis between camera and SQM data can be further developed into an automated event detection system, flagging periods of cloud cover, aurora, or significant increases in artificial light pollution.

Applying this workflow to a network of cameras at different sites (urban, rural, coastal, latitudes) would allow for comparative studies of light pollution, atmospheric extinction, and sky colour trends over time.

Long-term data collection would enable the study of seasonal variations in sky brightness and colour, as well as the impact of weather events (e.g., Saharan dust, snow cover) on calibration.

Collaborating with international sky quality monitoring networks (e.g., Globe at Night, Dark Sky Association) would enhance the scientific value and impact of the data.

Bibliography

(2019). Washetdonker.nl. https://www.washetdonker.nl/data/index.php. Accessed: 03-07-2025.

(2021). Keep it dark website. https://www.interregnorthsea.eu/kid. Accessed: 03-07-2025.

(2023). Darker sky website. https://www.interregnorthsea.eu/darker-sky. Accessed: 03-07-2025.

Aubé, M., Roby, J., and Kocifaj, M. (2013). Evaluating potential spectral impacts of various artificial lights on melatonin suppression, photosynthesis, and star visibility. *PloS one*, 8(7):e67798.

Bessell, M. S. (2005). Standard photometric systems. *Annu. Rev. Astron. Astrophys.*, 43(1):293–336.

Calabretta, M. R. and Greisen, E. W. (2002). Representations of celestial coordinates in fits. *Astronomy & Astrophysics*, 395(3):1077–1122.

Cao, M., Xu, T., and Yin, D. (2023). Understanding light pollution: Recent advances on its health threats and regulations. *Journal of Environmental Sciences*, 127:589–602.

Cardiel, N., Zamorano, J., Carrasco, J. M., Masana, E., Bará, S., González, R., Izquierdo, J., Pascual, S., and Sánchez de Miguel, A. (2021). Rgb photometric calibration of 15 million gaia stars. *Monthly Notices of the Royal Astronomical Society*, 507(1):318–329.

Cinzano, P. (2005). Night sky photometry with sky quality meter. *ISTIL Int. Rep*, 9(1).

Ducati, J. R. (2002). VizieR Online Data Catalog: Catalogue of Stellar Photometry in Johnson's 11-color system. CDS/ADC Collection of Electronic Catalogues, 2237, 0 (2002).

Falchi, F., Cinzano, P., Elvidge, C. D., Keith, D. M., and Haim, A. (2011). Limiting the impact of light pollution on human health, environment and stellar visibility. *Journal of environmental management*, 92(10):2714–2722.

Falchi, F., Furgoni, R., Gallaway, T. A., Rybnikova, N. A., Portnov, B. A., Baugh, K., Cinzano, P., and Elvidge, C. D. (2019). Light pollution in usa and europe: The good, the bad and the ugly. *Journal of environmental management*, 248:109227.

Hänel, A., Posch, T., Ribas, S. J., Aubé, M., Duriscoe, D., Jechow, A., Kollath, Z., Lolkema, D. E., Moore, C., Schmidt, N., et al. (2018). Measuring night sky brightness: methods and challenges. *Journal of Quantitative Spectroscopy and Radiative Transfer*, 205:278–290.

Hearnshaw, J. B. (1996). *The measurement of starlight: two centuries of astronomical photometry*. Cambridge University Press.

Kannala, J. and Brandt, S. S. (2006). A generic camera model and calibration method for conventional, wide-angle, and fish-eye lenses. *IEEE transactions on pattern analysis and machine intelligence*, 28(8):1335–1340.

Kolláth, Z. (2010). Measuring and modelling light pollution at the zselic starry sky park. In *Journal of Physics: Conference Series*, volume 218, page 012001. IOP Publishing.

Kolláth, Z., Cool, A., Jechow, A., Kolláth, K., Száz, D., and Tong, K. P. (2020). Introducing the dark sky unit for multi-spectral measurement of the night sky quality with commercial digital cameras. *Journal of Quantitative Spectroscopy and Radiative Transfer*, 253:107162.

Lang, D., Hogg, D. W., Mierle, K., Blanton, M., and Roweis, S. (2010). Astrometry. net: Blind astrometric calibration of arbitrary astronomical images. *The astronomical journal*, 139(5):1782.

Nicotera, L. (2022). *Monitoring light Pollution–Calibration of SQMs using SUOMI satellite data*. PhD thesis.

Pun, C. S. J., So, C. W., Leung, W. Y., and Wong, C. F. (2014). Contributions of artificial lighting sources on light pollution in hong kong measured through a night sky brightness monitoring network. *Journal of Quantitative Spectroscopy and Radiative Transfer*, 139:90–108. Light pollution: Theory, modeling, and measurements.

Román, M. O., Wang, Z., Sun, Q., Kalb, V., Miller, S. D., Molthan, A., Schultz, L., Bell, J., Stokes, E. C., Pandey, B., et al. (2018). Nasa's black marble nighttime lights product suite. *Remote Sensing of Environment*, 210:113–143.

Sánchez de Miguel, A., Aubé, M., Zamorano, J., Kocifaj, M., Roby, J., and Tapia, C. (2017). Sky quality meter measurements in a colour-changing world. *Monthly Notices of the Royal Astronomical Society*, 467(3):2966–2979.

Sánchez de Miguel, A., Bará, S., Aubé, M., Cardiel, N., Tapia, C. E., Zamorano, J., and Gaston, K. J. (2019). Evaluating human photoreceptoral inputs from night-time lights using rgb imaging photometry. *Journal of imaging*, 5(4):49.

Vladimir, N. (2006). Light pollution, reproductive function and cancer risk. *Neuroendocrinology Letters*, 27(1-2).

Yin, J., Yao, Y., Qian, X., Liu, L., Chen, X., and Zhai, L. (2025). Calibration and applications of the all-sky camera at the ali observatory in tibet. *Monthly Notices of the Royal Astronomical Society*, 537(1):617–627.

Appendices

.1 Lauwersmeer Harbor and Zernike data

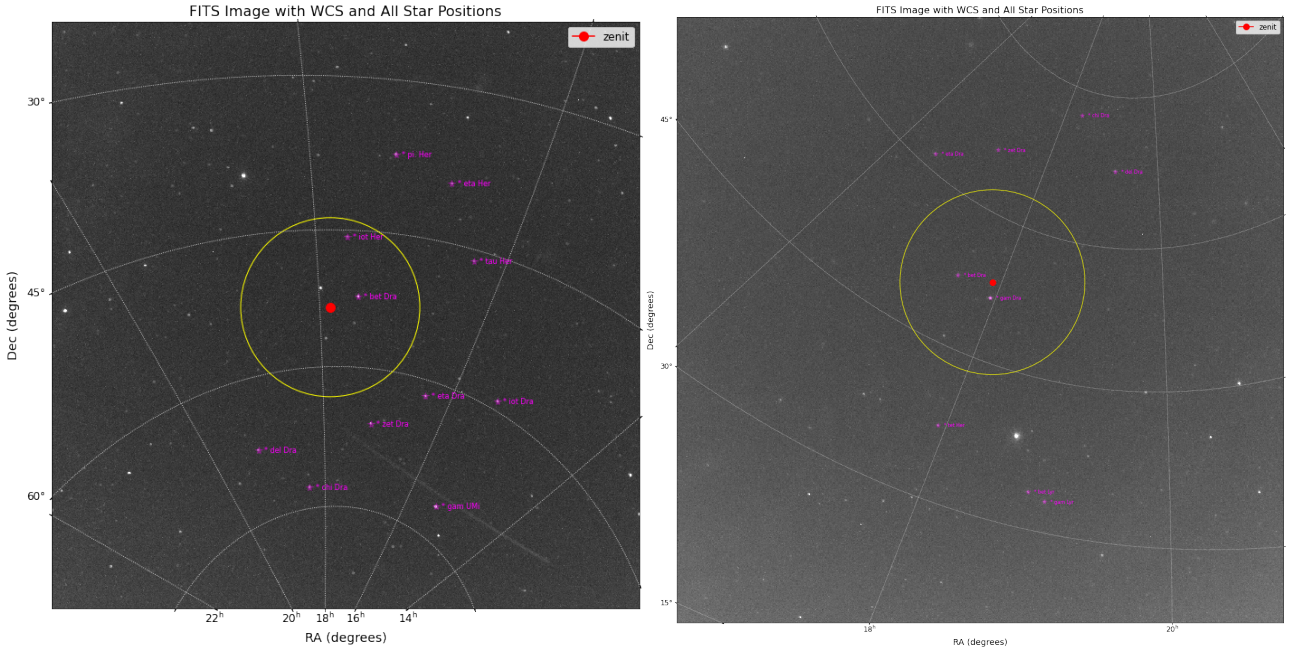

Lauwersmeer Harbor Zernike

Figure 25: Calibration star overview on June 20th

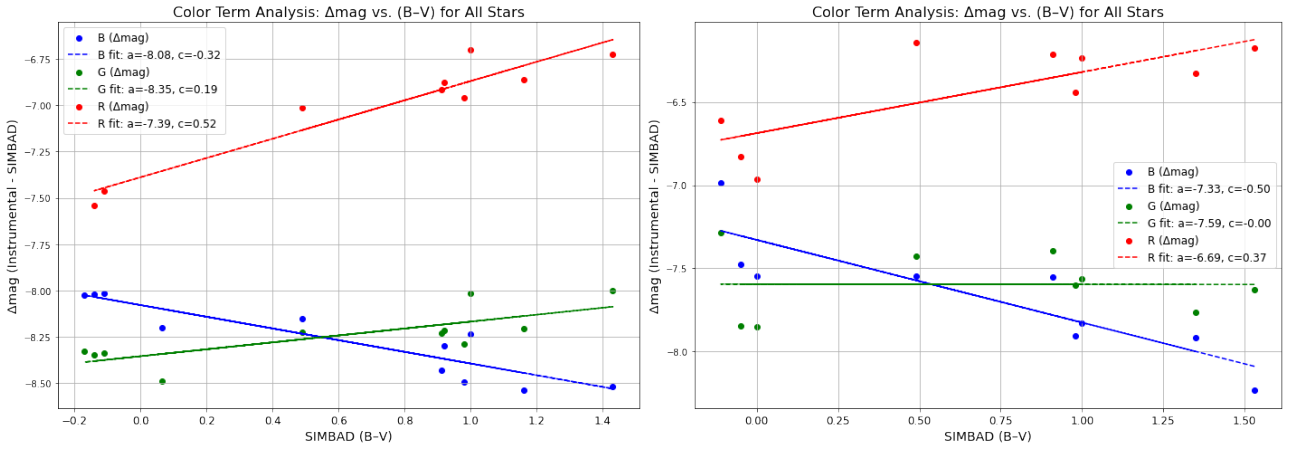

Lauwersmeer Harbor Zernike

Figure 26: Colour term calibration factor on June 20th

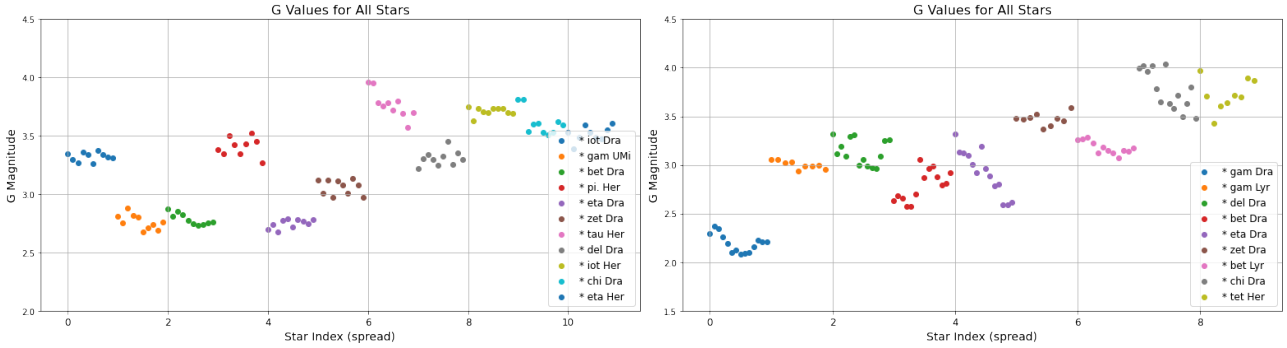

Lauwersmeer Harbor Zernike

Figure 27: Stellar Magnitudes on June 20th

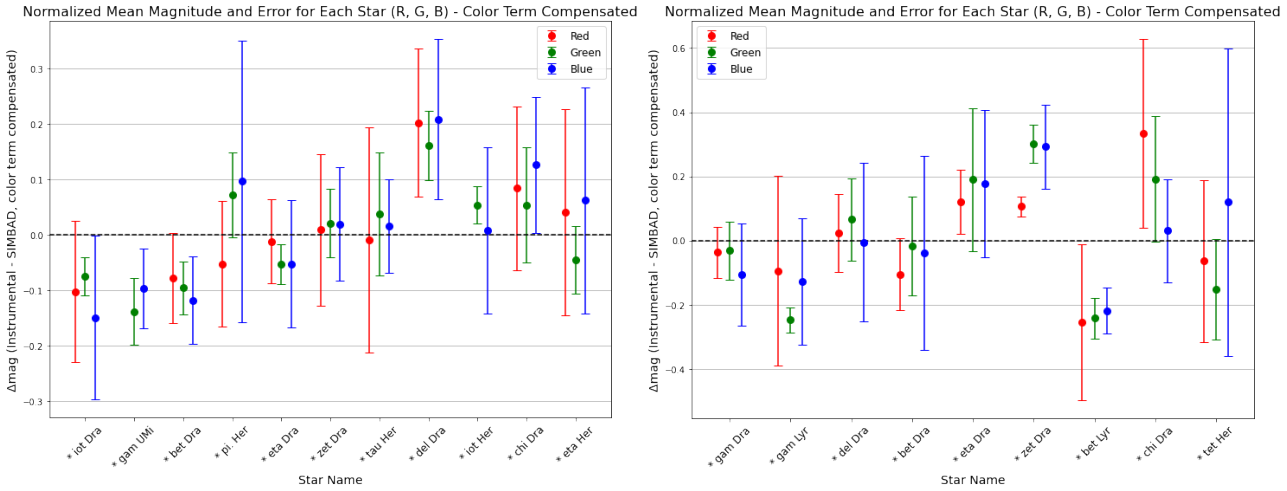

Lauwersmeer Harbor Zernike

Figure 28: Absolute magnitude of calibration stars on June 20th

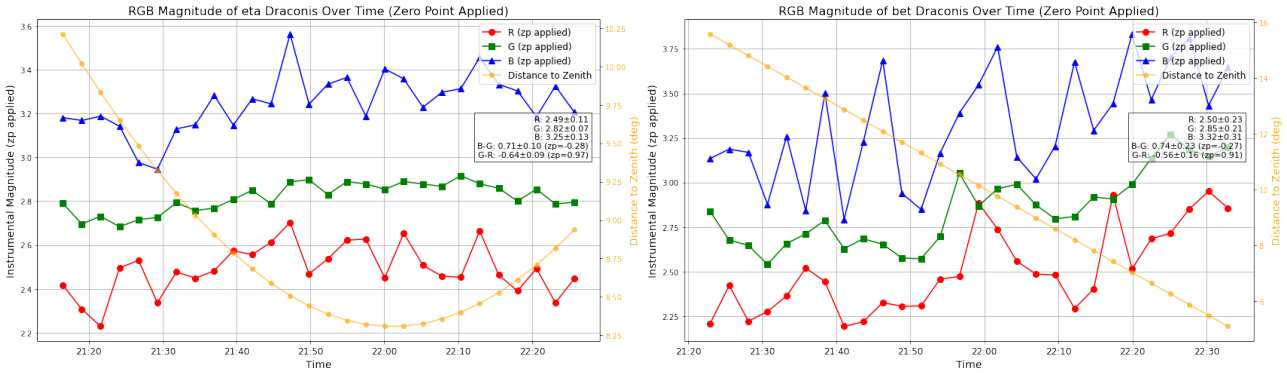

Lauwersmeer Harbor Zernike

Figure 29: Single star tracking on June 20th

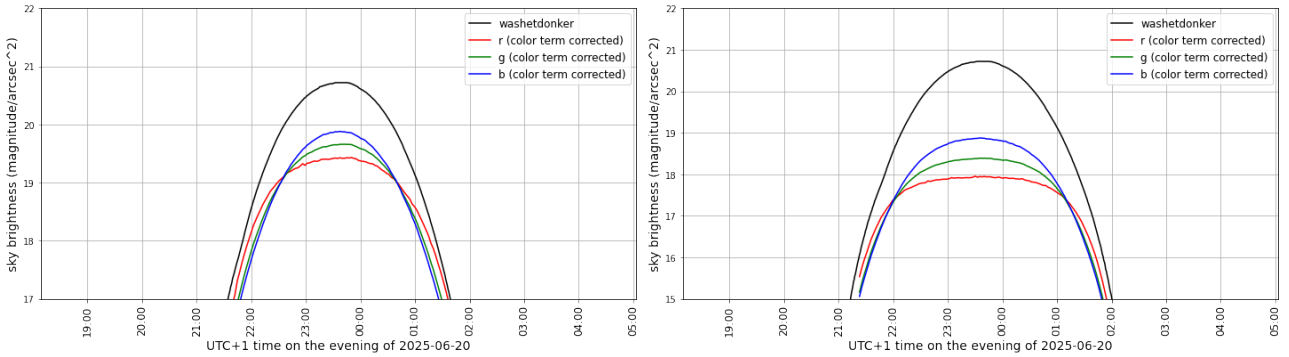

Lauwersmeer Harbor Zernike

Figure 30: Full night sky brightness profile of different colour bands and SQM data on June 20th

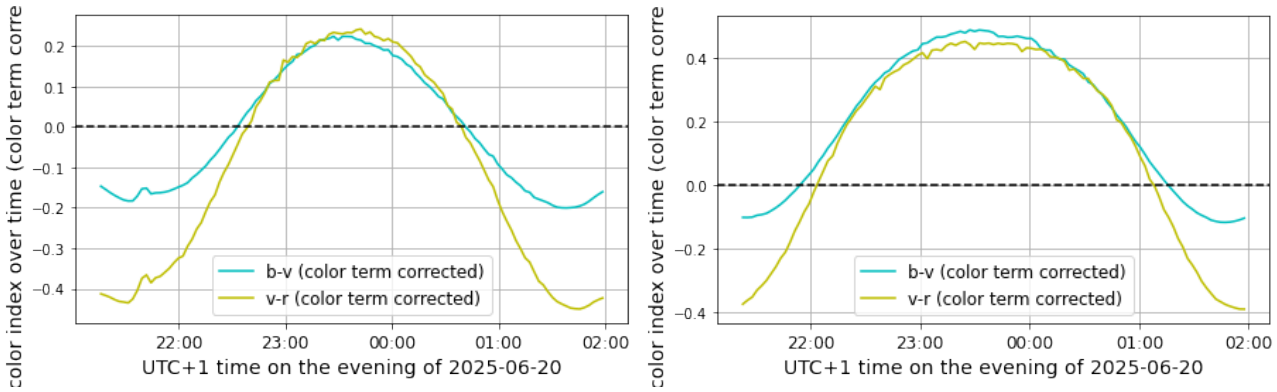

Lauwersmeer Harbor Zernike

Figure 31: Full night sky colour term on June 20th

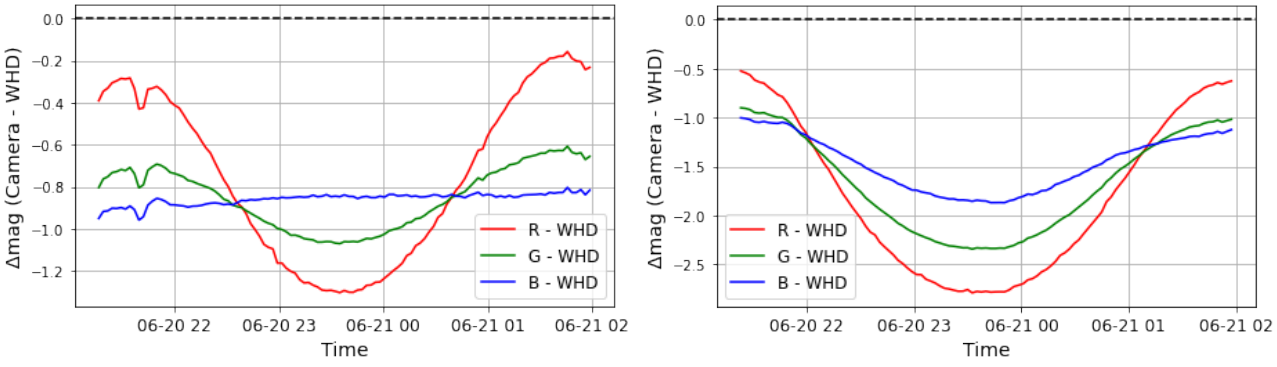

Lauwersmeer Harbor Zernike

Figure 32: Full night differences with SQM data on June 20th